Peptide-Derived Antagonists of the Urokinase Receptor. Affinity Maturation by Combinatorial Chemistry, Identification of Functional Epitopes, and Inhibitory Effect on Cancer Cell Intravasation†

Michael Ploug,*,‡ Søren Østergaard,§,|| Henrik Gårdsvoll,‡ Katherine Kovalski,⊥ Claus Holst-Hansen,‡ Arne Holm,§ Liliana Ossowski,⊥ and Keld Danø‡

Finsen Laboratory, Rigshospitalet, Strandboulevarden 49, DK-2100 Copenhagen Ø, Denmark, Chemistry Department, Veterinary and Agricultural University, Thorvaldsensvej 40, DK-1871 Frederiksberg C, Denmark, and Rochelle Belfer Chemotherapy Foundation Laboratory, Division of Medical Oncology, Department of Medicine, Mount Sinai School of Medicine, New York, New York 10029

Received April 2, 2001; Revised Manuscript Received July 12, 2001

ABSTRACT: The high-affinity interaction between urokinase-type plasminogen activator (uPA) and its glycolipid-anchored receptor (uPAR) plays an important role in pericellular plasminogen activation. Since proteolytic degradation of the extracellular matrix has an established role in tumor invasion and metastasis, the uPA−uPAR interaction represents a potential target for therapeutic intervention. By affinity maturation using combinatorial chemistry we have now developed and characterized a 9-mer, linear peptide antagonist of the uPA−uPAR interaction demonstrating specific, high-affinity binding to human uPAR ($K_d \approx 0.4$ nM). Studies by surface plasmon resonance reveal that the off-rate for this receptor−peptide complex is comparable to that measured for the natural protein ligand, uPA. The functional epitope on human uPAR for this antagonist has been delineated by site-directed mutagenesis, and its assignment to loop 3 of uPAR domain III (Met^{246}, His^{249}, His^{251}, and Phe^{256}) corroborates data previously obtained by photoaffinity labeling and provides a molecular explanation for the extreme selectivity observed for the antagonist toward human compared to mouse, monkey, and hamster uPAR. When human HEp-3 cancer cells were inoculated in the presence of this peptide antagonist, a specific inhibition of cancer cell intravasation was observed in a chicken chorioallantoic membrane assay. These data imply that design of small organic molecules mimicking the binding determinants of this 9-mer peptide antagonist may have a potential application in combination therapy for certain types of cancer.

Generation of pericellular proteolysis has an established role in the intensive tissue remodeling that accompanies cancer cell invasion and metastasis as well as nonmalignant processes such as wound healing and mammary gland involution (*1*−*5*). During the past decade experimental evidence has accumulated implicating an active involvement of the urokinase-type plasminogen activator (uPA)[1] and its receptor (uPAR) in the pathophysiology of cancer dissemination. First, in a number of different types of human cancer, elevated levels of uPAR, in either resected tumor tissue or in plasma, are correlated with a poor prognosis, providing a useful predictor of high-risk patients (*6*−*8*). Second, uPAR expression in disseminated tumor cells in the bone marrow of gastric cancer patients is correlated with an early relapse of the disease (*9*). Third, it has been demonstrated that the invasive potential of malignant human carcinoma cells is reduced significantly by anti-sense targeting of uPAR expression (*10*), and these cells thereby enter a state of prolonged dormancy (*11*, *12*). Finally, reductions in angiogenesis, primary tumor growth, or metastasis have been reported in various in vivo models using intervention

† This work was supported by the Danish Cancer Society, the NOVO-Nordisk Foundation, the Lundbeck Foundation, Harboefonden, Plasmidfonden, Dansk Kræftforskningsfond, Kong Christian IX og Dronning Louises Jubilæumslegat, Anna og Jakob Jakobsens Legat, U.S. Public Health Service Research Grant CA-40578, and the Samuel Waxman Cancer Research Foundation.

* To whom correspondence should be addressed. Tel: +45-35455706. Fax: +45-35385450. E-mail: m-ploug@finsenlab.dk.

‡ Finsen Laboratory, Rigshospitalet.

§ Chemistry Department, Veterinary and Agricultural University.

|| Present address: NOVO Nordisk A/S, Novo Allé 6B, DK-2880 Bagsvaerd, Denmark.

⊥ Department of Medicine, Mount Sinai School of Medicine.

[1] Abbreviations: βA, β-alanine; ANS, 8-anilino-1-naphthalenesulfonate; ATF, amino-terminal fragment of uPA; CAM, chorioallantoic membrane; Cha, β-cyclohexylalanine; CHO, Chinese hamster ovary cells; Chp, β-cycloheptylalanine; Cpa, β-cyclopentylalanine; DMB, 2,3-dimethoxybenzylamine; HEp-3, human epidermoid carcinoma cells; GFD, epidermal growth factor-like domain of uPA; MALDI-MS, matrix-assisted laser desorption ionization mass spectrometry; MEA, 2-methoxyethylamine; Nal, 2-naphthylalanine; TRA, tryptamine; uPA, urokinase-type plasminogen activator; suPAR, soluble uPA receptor. Common amino acids are shown in one-letter code (capitals denoting L-chirality and lower case D-chirality). Amines and amino acids with unnatural side chains are shown in a three-letter code. Synthetic peptides are identified by an AE code, and in the text peptide positions are numbered sequentially from the NH_2 terminus using a three-letter code and a superscript number, i.e., Cha^2 or Trp^8 for AE105 (D-Cha-FsrYLWS).

10.1021/bi010662g CCC: $20.00
Published on Web 09/13/2001

strategies based on macromolecular antagonists of the uPA−uPAR interaction (*13*−*17*).

The glycolipid-anchored uPAR (*18*, *19*) not only confines plasminogen activation to the pericellular environment by its interaction with pro-uPA but also improves the kinetics of plasminogen activation per se due to an increased efficiency of the reciprocal activation of both zymogens (*20*). This potentiation has an absolute requirement for the cellular assembly of both pro-uPA and plasminogen, since it can be counteracted by uPAR antagonists or lysine analogues (*20*). Consequently, soluble complexes between pro-uPA and a truncated, recombinant uPAR do not acquire this enhancement in plasminogen activation (*20*−*22*). An equivalent functional synergy between uPA and uPAR has recently been demonstrated in vivo on pathogenic plasminogen activation in the skin of transgenic mice (*23*). Mice bearing double transgenes that target a combined overexpression of uPA and uPAR to the keratinocytes of basal epidermis and hair follicles develop dramatic cutaneous alterations, including alopecia, epidermal thickening, and subepidermal blistering. In contrast, mice bearing a single transgene for either protein have a normal skin phenotype, as do the double transgenic mice for uPAR combined with a catalytically inactive mutant of uPA (*23*).

Collectively, these data highlight the uPA−uPAR interaction as a promising target for a receptor-specific intervention therapy aimed at controlling pathogenic plasminogen activation in cancer patients. The functional epitope on uPA for high-affinity uPAR interaction ($K_d \approx 0.5$ nM) is contained entirely within its small growth factor-like module (GFD; 4−43). A continuous, hydrophobic patch in the Ω-loop of GFD harbors the surface-exposed "hot spot" residues (Tyr^{24}, Phe^{25}, Ile^{28}, and Trp^{30}) that are essential for uPAR binding (*24*−*27*). The topology of the corresponding functional epitope on uPAR is unknown, since the three-dimensional structure of uPAR is yet to be solved. However, the overall folding topology of the three individual domains of uPAR is likely to resemble those solved for other members of the three-fingered Ly6/uPAR/α-neurotoxin protein domain family (*28*, *29*). On the basis of site-directed mutagenesis part of the functional epitope for uPA binding has been localized to residues Arg^{53}, Leu^{55}, Tyr^{57}, and Leu^{66} in loop 3 of uPAR domain I (*26*, *30*). A collection of 15-mer linear peptide antagonists of the uPA−uPAR interaction have been identified by selection in a random phage-display library (*31*), the major receptor-binding determinants of which (i.e., Phe, Leu, and Trp) have several properties in common with the functional epitope on uPA (*32*, *33*). A photoaffinity-labeled derivative of one of these peptides has been shown to bind uPAR in structural proximity to the functional uPA-binding epitope (*33*, *34*).

In this study we have used affinity maturation by combinatorial chemistry to identify a nonnatural 9-mer peptide antagonist of the uPA−uPAR interaction having greatly improved receptor-binding kinetics. The functional epitopes on both peptide antagonist and uPAR have been determined by alanine replacements, providing a reasonable molecular basis for the observed species specificity of the antagonists. We also show that this peptide is biologically active and inhibits intravasation of human cancer cells in a chorioallantoic membrane assay.

EXPERIMENTAL PROCEDURES

Chemicals and Reagents. Soluble, recombinant human uPAR (1−283) and mouse uPAR (1−275) were expressed either in Chinese hamster ovary cells or in *Drosophila* S2 cells and purified from the media as described previously (*29*, *35*). Murine uPA was expressed in *Drosophila* S2 cells and purified using receptor affinity chromatography (Gårdsvoll, unpublished). Recombinant human pro-uPA expressed in *Escherichia coli* and the amino-terminal fragment (ATF; residues 6−135) were kindly provided by Drs. D. Saunders (Grünenthal, Germany) and A. Mazar (Abbott Laboratories, Chicago, IL), respectively. The growth factor-like domain of uPA (GFD; residues 4−43) was produced by endoproteinase Glu-C digestion of human uPA (Serono, Aubonne, Switzerland) and purified as described previously (*26*). The monoclonal anti-uPAR antibody R2 was produced as published (*36*). Human plasminogen was purified from fresh, frozen plasma. Endoproteinase Lys-C (EC 3.4.21.50) and recombinant *N*-glycosidase F (EC 3.2.2.18) were from Roche Molecular Biochemicals (Germany). The chromogenic plasmin substrate (Spectrozyme PL) was from American Diagnostica (Greenwich, CT). TentaGel S amine was from Rapp Polymere (Tübingen, Germany). COFAL-negative embryonated eggs were from Specific Pathogen-free Avian Supply (Norwich, CT).

Construction of Constrained Peptide and Peptidomimetic Solid-Phase Libraries. Peptide bead libraries were based on the "one-bead−one-peptide" approach (*37*). Peptide library synthesis was performed by standard Fmoc chemistry on TentaGel S amine resin, while synthesis of the peptidomimetic library comprising a mixture of peptide−peptoid hybrids was accomplished as published previously (*38*, *39*). At variable positions in the constrained motif defining the two libraries, complexity was created by the split and mix approach of the solid-phase bead support (*40*). The peptide library was constrained according to the following motif: X_{0-3}FXXYLWS, where capital letters are L-amino acids and X is selected randomly among the following 25 amino acids: D-Ala, D-Ser, D-Thr, D-Tyr, D-Asp, D-Glu, D-Lys, D-His, D-Arg, D-Asn, D-Gln, D-Pro, D-Leu, D-Val, D-Ile, D-Met, D-Phe, D-Trp, D-phenylglycine, L-Cha, Gly, *O*-benzyl-L-tyrosine, *O*-benzyl-L-hydroxyproline, N^{im}-benzyl-L-histidine, and β-2-naphthyl-L-alanine. The peptidomimetic library was constrained according to the following motif: D[L-Cha]-FsrXXXX, where lower case letters are D-amino acids and X is selected randomly among the following 12 amino acids and 13 amines: L-Tyr, L-Trp, L-Leu, L-Cha, D-Tyr, D-Trp, D-Leu, D-Cha, D-Phe, D-His, β-2-naphthyl-L-alanine, N^{im}-benzyl-L-histidine, 1-aminoindan, tryptamine, diphenylethylamine, 1-aminomethylnaphthalene, benzylamine, 2,3-dimethoxybenzylamine, 2-aminoethyl-2-pyridine, 2-(4-methoxy)-phenylethylamine, aminomethylcyclohexane, isobutylamine, 3,3-dimethylbutylamine, 1-butylamine, and 2-methoxyethylamine. To enable determination of chirality during microsequencing, when both L- and D-amino acids were present in the library, the L-amino acids were encoded with 10% leucine, while the corresponding D-amino acids were encoded with 10% norvaline (39).

Selection of uPAR-Binding Beads in Solid-Phase Libraries. Beads presenting uPAR-binding peptides were identified after incubation with 100 nM suPAR followed by a biotinylated

monoclonal anti-uPAR antibody (R2), streptavidin-conjugated alkaline phosphatase (Sigma), and its substrate 5-bromo-4-chloro-3-indolyl phosphate. The combinatorial libraries were screened by one of two methods. In the first method beads interacting with biotinylated R2 or streptavidin were initially cleared from the library by a prescreening before the actual screening with uPAR was performed. In the second method prescreening with biotinylated R2 and streptavidin alkaline phosphatase was developed with 5-bromo-4-chloro-3-indolyl phosphate and *p*-iodonitrotetrazolium violet, causing a brownish dyeing of the positive beads, whereas the final screening with suPAR was counterstained with 5-bromo-4-chloro-3-indolyl phosphate and nitroblue tetrazolium, yielding a blue-purple color. Blue-colored beads were picked from the library and subjected to microsequencing. All incubations with proteins were performed at room temperature and pH 7.4 in 50 mM Tris, 0.25 M NaCl, 0.1% (w/v) gelatin, 0.05% (v/v) Tween-20, and 0.02% NaN_3.

Peptide Synthesis and Purification. Free peptides were synthesized, HPLC-purified, and verified by mass spectrometry as described previously (*33*). The covalent "dimers" AE120, AE151, and AE152 were synthesized on a modified lysine scaffold having its ϵ-amino group prederivatized with β-alanine, thus creating a pseudosymmetrical dimer with respect to the α-carbon atom of lysine.

Construction, Expression, and Purification of uPAR Mutants. Soluble, intact human uPAR (residues 1−283) carrying defined single-site alanine mutations in uPAR domain I were produced as described previously (*30*). Likewise, alanine mutations in uPAR domain III were constructed in the pCI-neo/suPAR vector (*30*) using an upstream primer residing in domain II, a downstream primer located in the pCI-neo T3 region, and one mutagenic primer designed to contain at least 10 perfectly matched bases at both the 5′ and 3′ ends of the mutagenic site. The corresponding suPAR domain III mutant PCR fragments were cloned into genuine *Apa*I and *Eco*RI sites of the pCI-neo/suPAR depleted for wild-type domain III. Prior to transfection PCR-generated sequences of all constructs were confirmed by DNA sequencing. Stable transfection of Chinese hamster ovary cells with the respective expression vectors and purification of the secreted suPAR mutants from the conditioned media were performed as described previously (*30*).

Confirmation at the protein level of mutations introduced into domain III of uPAR was obtained by mass spectrometry. In brief, purified uPAR mutants (10 μg) were reduced and alkylated by incubation for 5 min at 90 °C in 4 μL of 6 M guanidine hydrochloride including 50 mM DTT, 5 mM EDTA, and 0.1 M Tris (pH 8.0), followed by addition of 1 μL of 0.5 M iodoacetamide at room temperature. Specific proteolytic cleavages of the unfolded polypeptide chains of the individual mutants were subsequently achieved by addition of 40 μL of H_2O containing 1 μg of endoproteinase Lys-C and incubation for 3 h at room temperature, followed by addition of 25 ng of *N*-glycosidase F and a further incubation overnight. MALDI-MS spectra for these enzyme digests were recorded after sample deposition in α-cyano-4-hydroxycinnamic acid using the sandwich approach (*41*). All masses determined for Lys-C fragments (residues 199−232 and 233−268) covering the region subjected to mutagenesis were consistent with those calculated for each mutant within a mass accuracy of $\pm$1 Da, when spectra were calibrated internally using the dimer of the matrix ions and a Lys-C-generated uPAR peptide located distantly from the mutagenesis sites (residues 8−43).

Real Time Binding Kinetics of Peptide Antagonists Measured by Surface Plasmon Resonance. The kinetics of the interactions between suPAR and various synthetic peptides were measured directly in real time by surface plasmon resonance using a BIAcore 2000 equipment (Pharmacia Biosensor, Uppsala, Sweden). One of the interaction partners (either receptor, uPA, or peptide) was covalently immobilized by amine coupling on a carboxymethylated dextran matrix (CM5 sensor chip) preactivated with *N*-hydroxysuccinimide/*N*-ethyl-*N*′-[3-(diethylamino)propyl]carbodiimide. For practical reasons, neuraminidase treatment of purified suPAR from CHO cells was required prior to its covalent immobilization onto the biosensor chip (*33*), but as published previously this did not affect its binding kinetics with the natural protein ligand, uPA (*42*). This treatment was not necessary for coupling of uPAR produced in *Drosophila* S2 cells, since these insect cells do not add sialic acid during glycosylation. Coupling was achieved by injection of either uPA or suPAR at 20 μg/mL in 10 mM sodium acetate, pH 5.0, at a flow rate of 5 μL min^{-1} for 6 min, resulting in a coupling yield between 1000 and 4000 resonance units. Synthetic peptides were immobilized exclusively by their NH_2 termini (since no internal lysines or cysteines are present) by injection of the relevant peptide at 500 μg/mL, giving a coupling yield of 200−1000 resonance units (depending on peptide size, solubility, and isoelectric point).

Sensorgrams (resonance units versus time) were recorded by the BIAcore 2000 at a flow rate of 10 μL min^{-1} at 5 °C, using several different concentrations of analyte (receptor or peptide) dissolved in running buffer [10 mM HEPES, 3 mM EDTA, 150 mM NaCl (pH 7.4), including 0.005% surfactant P-20]. Peptides were diluted in running buffer from a 5 mM stock solution in DMSO. Sensor chips were regenerated at the end of each run by injection of 0.1 M acetic acid containing 0.5 M NaCl.

Data obtained from parallel mock-coupled flow cells (derivatized in the presence of buffer only) served as blank sensorgrams for subtraction of changes in the bulk refractive index. The sensorgrams obtained were analyzed by nonlinear least squares curve fitting using BIAevaluation 3.1 software (Pharmacia Biasensor, Uppsala, Sweden) assuming single-site association and dissociation models.

Competition of the Interaction between ^{125}I-Labeled ATF and uPAR on Intact Cells with Synthetic Peptides. The human breast cancer derived cell line MDA-MB-231 BAG expressing high amounts of uPAR was propagated as described and used for cell-binding experiments (*43*). Cells were suspended in Eagle's MEM media supplemented with 5% (v/v) fetal calf serum before they were seeded in 24-well plates at a cell density of 10^5 cells/well. Wells without cells served as background estimates, i.e., measuring binding of ^{125}I-labeled ATF to plastic. Adherent monolayers of MDA-MB-231 BAG cells were washed twice in binding buffer [Eagle's MEM media supplemented with 5 mM HEPES (pH 7.4), Glutamax-1, and 0.1% (w/v) bovine serum albumin]. Prior to conducting the binding experiment, cells were briefly exposed to 50 mM glycine hydrochloride and 0.1 M NaCl (pH 3.0), followed by neutralization (0.5 M HEPES, 0.1 M

NaCl, pH 7.5) and washing in binding buffer to dissociate and remove the endogenous, receptor-bound uPA. Relevant competitors diluted in binding buffer were added in duplicate to wells and preincubated for 15 min at 37 °C before addition of ^{125}I-labeled ATF (1 nM) and subsequent incubation for 60 min at 4 °C. After being washed three times in binding buffer, cells were lysed in 1 M NaOH, and a defined aliquot thereof was subjected to γ-counting to calculate the amount of bound ATF.

Intravasation of Human Cancer Cells Using a Chicken Chorioallantoic Membrane Assay. Intravasation experiments were performed essentially as described (*4*). HEp-3 tumors were dissociated with collagenase, plated at high density (5×10^6 per flask) in DMEM with 10% fetal bovine serum, incubated for 3−4 days, detached, and replated at 3×10^6 cells per 100 mm dish. In some experiments, the cells were preincubated with 10 μM uPA antagonist AE152 to reduce endogenously receptor-bound uPA. The cells were then washed, detached with 2 mM EDTA in PBS, and resuspended in PBS without or with the antagonist, and 1×10^6 cells in 50 μL were inoculated onto chorioallantoic membranes (CAM) of 9-day-old embryos on which an artificial air sac was created inside an 8 mm Teflon ring. PBS or the peptide antagonist was reapplied at 12 h intervals, and after 50 h incubation the "lower CAMs" were removed and processed as described (*4*). The snap-frozen CAMs were crushed and lysed, and the genomic DNA was isolated using the Puregen DNA isolation kit as per manufacturer specifications. This DNA was used to quantify intravasation by PCR of human *Alu* sequences. The specific primers for human *Alu* sequences were *Alu* sense, 5′ ACG CCT GTA ATC CCA GCA CTT 3′, and *Alu* antisense, 5′ TCG CCC AGG CTG GAG TGC A 3′, which produced a band of 224 bp upon PCR amplification. The PCR was performed under the following conditions: 95 °C for 10 min, 95 °C for 30 s, 58 °C for 45 s, 72 °C for 45 s, and 72 °C for 10 min. The reaction mixture contained 1 μg of genomic DNA as template, 1 × PCR buffer, 1.5 mM $MgCl_2$, 50 μM dNTPs, 1 μM each of *Alu*-sense and anti-sense primers, 1−2 units of Amplitaq Gold, and 0.1 μCi of fresh [α-^{32}P]dCTP. The PCR products were electrophoresed on a 7% polyacrylamide gel at 100 V for 1 h, dried, and exposed to film at −80 °C. The bands were quantified by densitometric scanning using GelScan XL (Pharmacia, Sweden).

To measure the capacity of the HEp-3 cells to support plasminogen activation, cells were harvested with 2 mM EDTA in PBS from cell cultures treated as for the intravasation experiments. These cells were washed, counted, and resuspended in 100 μL of PBS containing 5 μg of plasminogen. Such suspensions were incubated at 37 °C for 30 min before supernatants were collected by centrifugation. The generated plasmin activities were measured by mixing aliquots of the collected supernatants with 15 μg of chromogenic plasmin substrate in a total volume of 125 μL [0.1 M Tris, pH 8.1, containing 0.1% (v/v) Triton X-100]. The plate was incubated at 37 °C and read at 410 nm by a Dynatech MR 700 multiwell plate reader. The background of plasminogen without sample was subtracted.

Miscellaneous Analyses. uPAR-mediated enhancement of 8-anilino-1-naphthalenesulfonate (ANS) fluorescence was recorded by a Perkin-Elmer LS-5 spectrofluorometer with excitation and emission wavelengths set at 386 and 470 nm, respectively. Titration of this uPAR-specific ANS fluorescence by synthetic peptides was performed essentially as described for a similar titration using monoclonal anti-uPAR antibodies (*44*).

Table 1: Sequences Selected during Screening of a Combinatorial Solid-Phase Peptide Library with Purified Recombinant uPAR[a]

peptide library: $X_{0-3}FXXYLWS$	
group I	group II
e-Cha-F-s-y-Y-L-W-S	r-r-F-h-q-Y-L-W-S
d-Cha-F-s-r-Y-L-W-S	r-n-F-h-r-Y-L-W-S
t-Cha-F-s-r-Y-L-W-S	r-r-F-h-h-Y-L-W-S
n-s-Cha-F-s-r-Y-L-W-S	a-r-F-h-r-Y-L-W-S
s-p-Cha-F-s-y-Y-L-W-S	r-n-F-s-t-Y-L-W-S
v-n-Cha-F-s-y-Y-L-W-S	r-h-r-F-q-n-Y-L-W-S
	h-n-r-F-t-r-Y-L-W-S
motif A: x-**Cha**-**F**-**s**-x-Y-**L**-**W**-S	

[a] The design of this peptide library gives rise to a theoretical complexity of 9.9×10^6, while the actual size of the present library is 3×10^6. The motif used to constrain the library is underlined. Peptides in group I are considered to represent peptides binding specifically to uPAR, whereas peptides in group II are thought to interact with the detection system, i.e., the biotinylated, monoclonal anti-uPAR antibody R2. L-Amino acids are shown in capital letters and D-amino acids in lower case letters. Cha is β-cyclohexyl-L-alanine.

RESULTS AND DISCUSSION

Selection of uPAR-Binding Peptides and Peptidomimetics by Combinatorial Chemistry. Initial screening in naive octamer and decamer combinatorial peptide libraries for uPAR-binding sequences proved essentially negative, presumably due to the limited complexity of the employed "one-bead−one-sequence" libraries. A 15-mer peptide antagonist of the uPA−uPAR interaction previously identified by phage-display technology (*31*) was therefore chosen as a template for the tailoring of a constrained solid-phase peptide library. The minimal sequence of this 15-mer peptide required for maintenance of its nanomolar affinity for uPAR was initially determined by consecutive truncations at the COOH and NH_2 termini. Residues critical for the binding properties of the resultant decapeptide (SLNFSQYLWS) were identified by alanine replacement as published previously (*33*). A solid-phase combinatorial peptide library was subsequently synthesized and constrained in accordance to the derived consensus motif: X_{0-3}**F**XXY**LW**S, where X represents the choice between 25 different amino acids and the letters in bold highlight the residues critical for uPAR binding. A limited number of beads stained positive when this peptide library was probed with purified recombinant soluble uPAR. Edman sequencing of 13 of these uPAR positive beads led to the extension of the consensus for uPAR-binding peptides, since 6 of the selected peptides defined the following motif: x-**Cha**-**F**-**s**-x-Y-**L**-**W**-S (motif A in Table 1). The remaining 7 peptides were considered to interact with the biotinylated detection antibody (R2), despite precleaning of the library, since they contained several histidine and/or arginine residues. The latter assumption was further substantiated by kinetic analysis for one of these peptides, which did not present any measurable binding to immobilized uPAR (AE104, Table 3). To target the COOH-terminal region, kept invariable during the first screening, a second library was generated according to the following consensus motif: D-**Cha**-**F**-**s**-r-X-X-X-X, where X represents the choice

Table 2: Sequences Selected during Screening of a Combinatorial Solid-Phase Peptidomimetic Library with Purified Recombinant uPAR[a]

peptidomimetic library: DChaFsrXXXX	
group I	group II
D-Cha-F-s-r-L-L-W-h	D-Cha-F-s-r-DMB-f-TRA-MEA
D-Cha-F-s-r-Cha-L-W-l	D-Cha-F-s-r-DMB-f-AMN-MEA
D-Cha-F-s-r-L-L-W-h	D-Cha-F-s-r-DMB-f-TRA-?[b]
D-Cha-F-s-r-Y-L-Nal-h	D-Cha-F-s-r-DMB-f-AMN-MEA
	D-Cha-F-s-r-DMB-f-DMB-l
	D-Cha-F-s-r-DMB-f-DMB-Y
motif B: x-**Cha**-**F**-**s**-x-**DMB**-**f**-**Ara**-x	

[a] This peptidomimetic library has a theoretical complexity of 0.4×10^6, while the actual size is 1×10^6; i.e., it contains 2.5 library equivalents, which is the reason for the occurrence of identical sequences in the table. The motif used to constrain the library is underlined. Peptides in group I comply to the consensus motif A found in Table 1, whereas group II entirely contains peptidomimetics defining an extended consensus motif B. L-Amino acids are shown in capital letters and D-amino acids in lower case letters. Cha is β-cyclohexyl-L-alanine, Nal is β-2-naphthyl-L-alanine, DMB is 2,3-dimethoxybenzylamine, TRA is tryptamine, MEA is 2-methoxyethylamine, AMN is 1-aminomethylnaphthalene, and Ara is an aromatic amine. [b] Residue not determined during microsequencing.

Table 3: Binding Kinetics for the Interaction between Peptides and Peptidomimetics Selected by Combinatorial Chemistry and Immobilized uPAR As Measured by Surface Plasmon Resonance[a]

code	sequence	on-rate (10^5 M^{-1} s^{-1})	off-rate (10^{-4} s^{-1})	K_d (10^{-9} M)
AE78	AEPMPHSLNFSQYLWYT[b]	11	91	8.3
AE68	SLNFSQYLWS[b]	13	241	19
AE100	e-Cha-F-s-y-Y-L-W-S	4.6	7.0	1.5
AE101	d-Cha-F-s-r-Y-L-W-S	5.8	5.4	0.93
AE108	t-Cha-F-s-r-Y-L-W-S	5.9	3.7	0.63
AE104	a-r-F-h-r-Y-L-W-S	ND[c]	ND[c]	ND[c]
AE124	D-Cha-F-s-r-DMB-f-TRA-MEA	11	56	5.1
AE126	D-Cha-F-s-r-DMB-f-AMN-MEA	2.4	3.7	1.5
AE129	D-Cha-F-s-r-DMB-f-DMB-l	4.2	5.4	1.3
AE131	D-Cha-F-s-r-Y-L-Nal-h	2.5	5.6	2.2
AE128	D-Cha-F-s-r-MEA-DMB-f-AMN	ND[c]	ND[c]	ND[c]
GFD	residues 4−43	2.5	1.7	0.68
ATF	residues 6−135	3.8	1.3	0.34
pro-uPA	residues 1−411	2.6	0.81	0.31

[a] The interaction between immobilized suPAR and the respective ligands was measured at 5 °C for serial 2-fold dilutions of the soluble peptides/peptidomimetics (ranging from 1 μM to 8 nM) and the receptor-binding derivatives of uPA (ranging from 200 to 2 nM). Shown are the means for k_{on} and k_{off} determinations from 6 to 30 different measurements (experimental standard deviations ranged between 30% and 50%). The equilibrium dissociation constant (K_d) is calculated from the ratio of the experimentally determined rate constants, k_{off}/k_{on}. Amino acids and amines are abbreviated as described in the legend to Table 2. [b] Peptide AE78 contains the 15-mer uPAR-binding peptide originally selected as clone 20 by bacteriophage display (*31*) as well as a two-residue amino-terminal extension derived from the phage sequence. AE68 is a truncated uPAR-binding version of AE78 (*33*, *34*). [c] No binding was detected using peptide concentrations up to 10 μM.

between 13 different amines and 12 D- or L-amino acids. Again, a limited number of beads stained positive after incubation with purified uPAR, and subsequent microsequencing revealed that they belonged to one of two consensus patterns: the first group contained peptides, which comply to motif A, whereas the second group contained peptidomimetics defining motif B: x-**Cha**-**F**-**s**-x-**DMB**-**f**-**Ara**-x (Table 2).

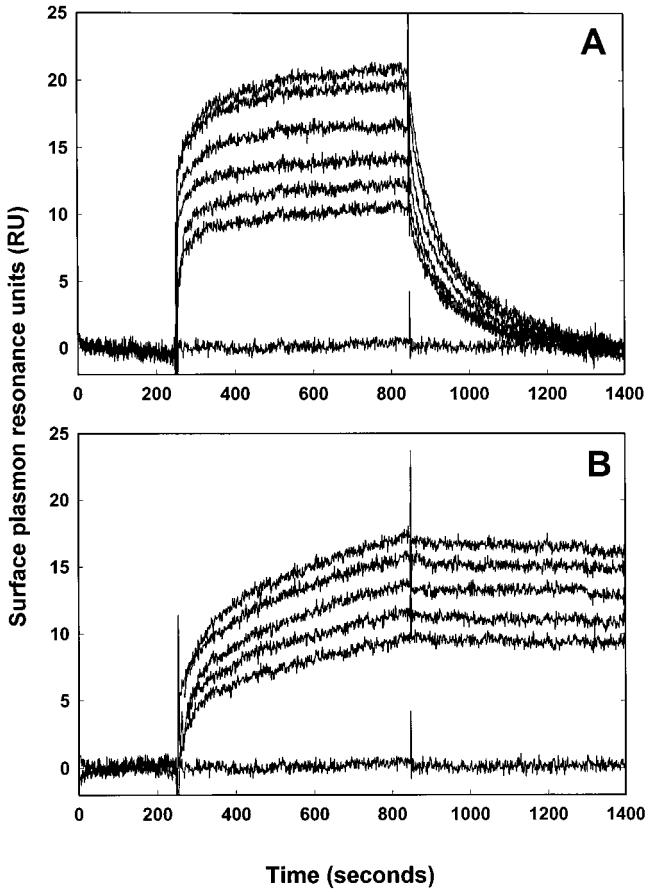

FIGURE 1: Real time binding kinetics between synthetic peptides and immobilized uPAR measured by surface plasmon resonance. The association and dissociation profiles for the interactions between immobilized uPAR (2900 RU) and serial 2-fold dilutions of either the 15-mer parent peptide selected by phage display (AE78, panel A) or the 9-mer affinity-matured peptide selected by combinatorial chemistry (AE105, panel B) were recorded by surface plasmon resonance at 5 °C. The highest peptide concentration tested is 1 μM for AE78 and 250 nM for AE105 (top curve in each panel).

Receptor-Binding Properties of the Free Peptides Identified by Combinatorial Chemistry. To evaluate the uPAR-binding properties of sequences selected from the constrained solid-phase libraries, a collection of the corresponding free peptides and peptidomimetics were synthesized, and their interaction with immobilized uPAR was measured in real time by surface plasmon resonance. As shown in Table 3, the derived equilibrium dissociation constants (K_d) are in the subnanomolar range, thus demonstrating greatly improved receptor-binding affinity compared to the parent peptide (AE68). These improvements are primarily governed by a substantial reduction in k_{off} (up to 65-fold; Figure 1), some of which are now approaching that for the natural protein ligand, pro-uPA (Table 3). However, the corresponding k_{on} values were also reduced by 2−3-fold, yielding an overall improvement in the affinity for uPAR of 15−30-fold. The differential contribution of the two rate constants to the improved affinity may be related to the experimental design, which favors off-rate selection due to the extensive washing steps after the library was probed with purified receptor. It has been reported previously that affinity maturations of monoclonal antibodies generally lead to an optimized high affinity through larger improvements in k_{off} than in k_{on} (*45*−*47*).

Table 4: Identification of Structures in Selected Peptides Important for uPAR-Binding Properties[a]

code	sequence	on-rate (10^5 $M^{-1}s^{-1}$)	off-rate (10^{-4} s^{-1})	K_d (10^{-9} M)
AE101	d-Cha-F-s-r-Y-L-W-S	5.8	5.4	0.93
AE105	**D**-Cha-F-s-r-Y-L-W-S	6.4	2.3	0.36
AE106	D-Cha-F-**S**-r-Y-L-W-S	12	31	2.6
AE110	D-Cha-F-s-**R**-Y-L-W-S	4.2	2.8	0.67
AE112	D-**F**-F-s-r-Y-L-W-S	14	26	1.9
AE113	D-**N**-F-s-r-Y-L-W-S	ND[b]	ND[b]	ND[b]
AE116	D-Cha-F-s-r-**G**-Y-L-W-S	ND[b]	ND[b]	ND[b]
AE133	KGSGG-D-Cha-F-s-r-Y-L-W-S	5.4	2.5	0.46
AE133*	KGSGG-D-Cha-F-s-r-Y-L-W-S	0.19	2.8	15
AE134	KGSGG-D-Cha-F-s-r-Y-L-W-**A**	3.0	3.9	1.3
AE135	KGSGG-D-Cha-F-s-r-Y-L-**A**-S	ND[b]	ND[b]	ND[b]
AE136	KGSGG-D-Cha-F-s-r-Y-**A**-W-S	ND[b]	ND[b]	ND[b]
AE137	KGSGG-D-Cha-F-s-r-**A**-L-W-S	4.1	9.8	2.4
AE138	KGSGG-D-Cha-F-s-**a**-Y-L-W-S	5.0	12	2.4
AE139	KGSGG-D-Cha-F-**a**-r-Y-L-W-S	13	6.3	0.48
AE145	KGSGG-D-Cha-F-**A**-r-Y-L-W-S	ND[b]	ND[b]	ND[b]
AE140	KGSGG-D-Cha-**A**-s-r-Y-L-W-S	ND[b]	ND[b]	ND[b]
AE141	KGSGG-D-**A**-F-s-r-Y-L-W-S	0.41	72	176
AE142	KGSGG-**A**-Cha-F-s-r-Y-L-W-S	5.6	5.7	1.0
AE143	KGSGG-D-**Chp**-F-s-r-Y-L-W-S[c]	6.3	4.3	0.68
AE144	KGSGG-D-**Cpa**-F-s-r-Y-L-W-S[c]	7.4	5.2	0.70
AE164	KGSGG-D-**F**-F-s-r-Y-L-W-S	1.5	36	24
AE164*	KGSGG-D-**F**-F-s-r-Y-L-W-S	0.20	27	135
AE120	[D-Cha-F-s-r-Y-L-W-S]$_2$-βA-K[c]	5.1	0.66	0.13
AE120*	[D-Cha-F-s-r-Y-L-W-S]$_2$-βA-K[c]	0.74	0.34	0.46
AE151	[r-W-D-Cha-S-L-s-F-Y]$_2$-βA-K[c]	ND[b]	ND[b]	ND[b]

[a] Real time binding kinetics were measured by surface plasmon resonance at 5 °C for the interaction between immobilized uPAR and the free peptides (serial 2-fold dilutions ranging from 1 μM to 8 nM), except for AE133*, AE120*, and AE164*, in which case the peptides were covalently immobilized via their NH_2 termini and the interaction was measured using suPAR in solution (serial 2-fold dilutions ranging from 200 to 2 nM). [b] No binding detected using peptide concentrations up to 10 μM. [c] Chp is β-cycloheptyl-L-alanine, Cpa is β-cyclopentyl-(L/D)-alanine, and βA is β-L-alanine.

The screening of the second sublibrary did not lead to any additional improvements in the affinity of the selected peptidomimetics (Table 3), but binding was still sequence specific, since scrambling the COOH-terminal part of one selected peptidomimetic rendered it nonbinding (AE126 versus AE128, Table 3). Although not displaying an improved affinity, these peptidomimetics may be useful in the design of a receptor-specific tumor therapy, since they are inherently more resistant to proteolysis than the sequences selected from the peptide library (data presented later, Figure 3).

Identification of Pharmacophores Involved in uPAR Binding. To explore the functional impact of each amino acid side chain on the high-affinity interaction with uPAR, one of the selected nonapeptides (AE101, Table 3) was subjected to a systematic, single-site replacement strategy (Table 4). Some of these derivatives were also extended at the NH_2 terminus (AE133 to AE145) with the dual purpose of increasing their mass, to improve the signal-to-noise ratio during surface plasmon resonance analysis, and allowing the peptides to be immobilized directly on the sensor chip, enabling the reverse interaction analysis using soluble uPAR as analyte. The NH_2-terminal sequence extension did not alter the uPAR-binding properties (AE105 versus AE133, Table 4).

Kinetic analysis by surface plasmon resonance for derivatives of AE133, carrying alanine substitutions preserving the original chirality at each individual position, clearly demonstrates the critical contribution of the hydrophobic amino acid side chains of L-Cha^2 (AE141), L-Phe^3 (AE140), L-Leu^7 (AE136), and L-Trp^8 (AE135) for the high-affinity interaction with immobilized uPAR (Table 4). Additional substitutions of L-Cha^2 revealed that the length of the saturated, cycloalkane side chain could be either increased (AE143) or decreased (AE144) by one carbon atom without affecting its interaction with uPAR, but introduction of L-Phe, the equivalent aromatic analogue of L-Cha, led to a more than 10-fold increase in k_{off} for the interaction with immobilized uPAR (AE112 versus AE105 and AE164 versus AE133).

Alanine replacements of L-Asp^1 (AE142), D-Arg^5 (AE138), L-Tyr^6 (AE137), or L-Ser^9 (AE134) had only minor effects on the measured k_{off} of such uPAR complexes. Unexpectedly, substitution of D-Ser^4 with D-Ala had very little effect on the peptide interaction with immobilized uPAR (AE139 versus AE133, Table 4) even though D-Ser was exclusively selected at this position in the combinatorial library (Table 1). Replacement of D-Ser^4 with either L-Ser (AE106) or L-Ala (AE145), however, significantly increases the k_{off} for such uPAR complexes, highlighting the importance of the correct chirality at position 4 in the peptide. A comparison between AE105 and AE116 reveals that the distance between the hydrophobic pharmacophores L-Cha^2/L-Phe^3 and L-Leu^7/L-Trp^8 also is critical for the antagonist properties of AE105 (Table 4).

Finally, we synthesized a pseudosymmetrical "covalent dimer" of AE105 onto a lysine scaffold. For as yet unknown reasons this derivative (AE120) exhibited an additional 3−4-fold reduction in k_{off} compared to AE105 and AE133 (Table 4). A scrambled version of AE120 did not present any measurable binding to uPAR (AE151; Table 4).

These kinetic data using the peptides as analytes were validated by determining k_{off} in a reverse experimental setup, in which the interactions between immobilized peptides and soluble uPAR revealed comparable k_{off} rates (AE133*, AE120*, and AE164*, Table 4). Although k_{off} was comparable, the k_{on} rates were significantly impaired, as should be anticipated for steric reasons when measuring the interaction between a relatively small ligand immobilized onto a dextran matrix and a macromolecular receptor in solution. As a final quality check on these kinetic data, k_{off} values for complexes between uPAR and either AE133 or AE164 were determined in solution by amide hydrogen−deuterium exchange and isotope-resolved mass spectrometry,[2] and these were concordant with those determined for the equivalent complexes using surface plasmon resonance (data not shown).

Inhibitory Properties of Affinity-Matured Peptides on the uPA−uPAR Interaction. Binding of 8-anilino-1-naphthalenesulfonate (ANS) to a surface-exposed hydrophobic patch on uPAR leads to an enhancement and blue shift in ANS fluorescence and monitors the availability of a high-affinity binding site for uPA (*44*). As shown in Figure 2A, the affinity-matured peptide AE105 titrates this uPAR-mediated enhancement of ANS fluorescence with a 1:1 stoichiometry, as do the natural protein ligands ATF and GFD. Abolition

[2] T. D. Jørgensen, H. Gårdsvoll, A. Holm, K. Danø, P. Roepstorff, and M. Ploug,manuscript in preparation.

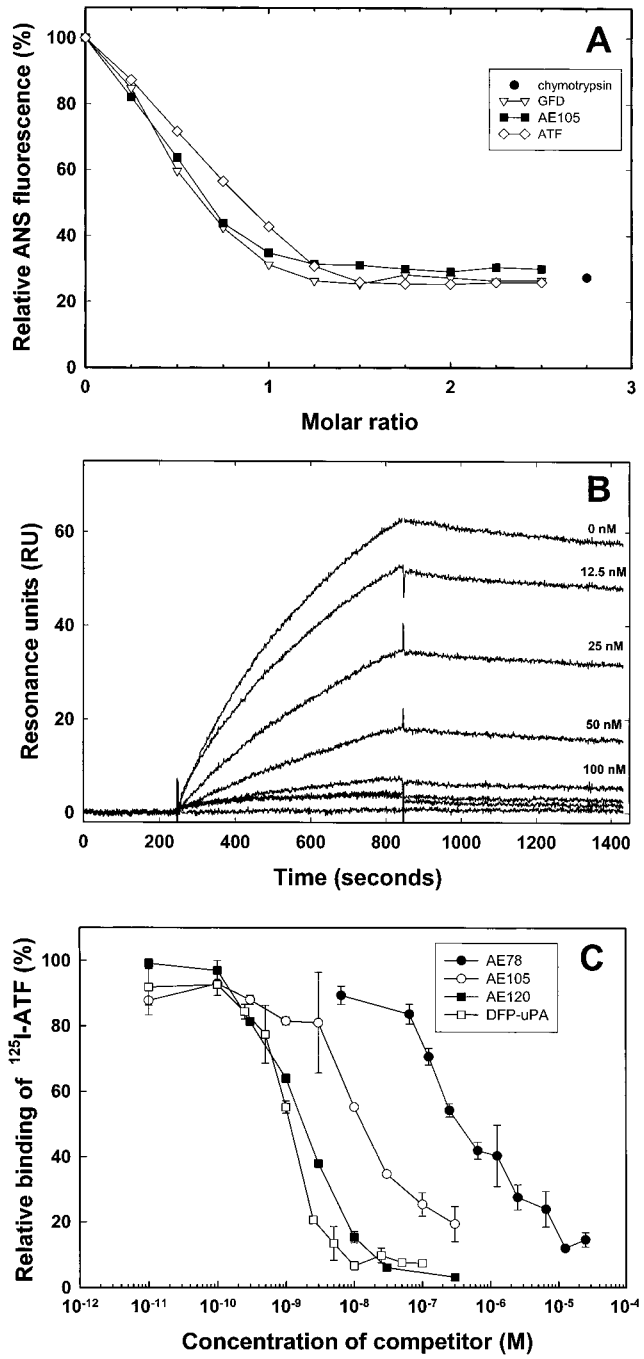

FIGURE 2: Antagonist effect of the affinity-matured peptides. Panel A: Titration of uPAR-mediated enhancement of ANS fluorescence by AE105, GFD, and ATF. The relative fluorescence emission of 10 μM ANS and 2 μM uPAR was measured as a function of increasing concentration of the respective ligands at 470 nm with excitation at 386 nm. Also shown is the decrease in ANS fluorescence observed as a consequence of specific enzymatic cleavage of the linker region between uPAR domains I and II by chymotrypsin. Panel B: Inhibition of the uPA−uPAR interaction by AE105 as measured in real time by surface plasmon resonance. The interaction between immobilized uPA (1200 RU) and 50 nM uPAR preincubated with serial 2-fold dilutions of AE105 (400−12.5 nM) was recorded at 5 °C by a BIAcore 2000. Panel C: Competition from synthetic peptides on the cellular binding of ATF. Acid-treated MDA-MD-231 BAG cells were preincubated for 15 min at 37 °C with various concentrations of unlabeled AE120, AE105, AE78, and DFP-uPA. The relative binding of ATF is shown as a function of the concentration of the various competitors.

of the high-affinity binding site for uPA by specific chymotryptic hydrolysis after Tyr^{87} (*44*) is also accompanied by a similar reduction in the ANS fluorescence, having an end point comparable to that obtained after titration with AE105, GFD, or ATF (Figure 2A). The hydrophobic patch exposed on unligated uPAR is therefore specifically targeted by this small synthetic peptide ligand in a manner indistinguishable from that of the natural protein ligand.

Two additional experiments were performed in order to directly measure whether AE105 and uPA compete for binding to uPAR. In the first experiment, we used surface plasmon resonance to record the binding kinetics between immobilized uPA and 50 nM uPAR preincubated with various concentrations of AE105 (Figure 2B). Since this concentration of uPAR far exceeds the K_d determined for the uPAR−AE105 interaction (0.35 nM), this experiment mimics an "active site titration" by which the availability of an unoccupied, high-affinity binding site for uPA on uPAR is determined. As shown in Figure 2B, AE105 neutralizes the uPA-binding properties of uPAR with a binding stoichiometry close to 1:1, in agreement with its effect on the specific ANS fluorescence (Figure 2A). A similar titration profile was obtained when GFD was used as competitor (data not shown). Being a competitive inhibitor, the presence of AE105 does not affect the stability of the uPA−uPAR complexes, and accordingly injections of high concentrations of AE105 fail to promote the dissociation of preformed uPA−uPAR complexes on the biosensor surface (data not shown).

In the second experiment, we determined the competition of various unlabeled peptide inhibitors for the interaction between ^{125}I-labeled ATF (1 nM) and the human breast cancer derived cell line MDA-MD-231 BAG. As shown in Figure 2C, the synthetic peptide AE120 is almost as efficient as DFP-inactivated uPA in competing the interaction between ^{125}I-labeled ATF and cell surface uPAR, yielding IC_{50} values of 2 nM for AE120 and 1 nM for DFP-uPA. These values compare favorably with the K_d's for their interaction with immobilized uPAR determined by surface plasmon resonance (0.13 nM for AE120 and 0.31 nM for pro-uPA). The potency of AE105 is moderately reduced compared to AE120 (IC_{50} values of 20 versus 2 nM), whereas the original 15-mer phage-display peptide AE78 demonstrates a rather poor inhibitory potential ($IC_{50} \approx 500$ nM). The latter two peptides may, however, have suffered an additional penalty in this assay, since they are expected to be the more susceptible to proteolytic degradation during the preincubation with cells for 15 min at 37 °C.

To further address the "biological stability" of selected antagonists experimentally, these were preincubated at 37 °C for 24 h in undiluted mouse serum. The impact of this treatment on the functional integrity of the antagonists was subsequently assessed by measuring their inhibitory properties in the cellular binding assay using MDA-MD-231 BAG cells (Figure 3). As anticipated from their chemical structures, the linear peptides AE78 and AE105 with unprotected COOH termini were severely degraded during the preincubation in mouse serum, whereas the inhibitory activities of the peptidomimetic AE126 and the covalent dimer AE120 were almost refractory to this treatment (Figure 3).

Species Specificity of the Antagonists. A pronounced species specificity exists in the uPA−uPAR interaction with little cross-reactivity observed between human and murine proteins (*32*, *48*). This property has a bearing on the practical

Table 5: Species Selectivity of the uPA−uPAR Interaction between Man and Mouse Assessed by Surface Plasmon Resonance[a]

	human uPAR			mouse uPAR		
	k_{on} (10^4 s^{-1} M^{-1})	k_{off} (10^{-5} s^{-1})	K_d (10^{-9} M)	k_{on} (10^4 s^{-1} M^{-1})	k_{off} (10^{-5} s^{-1})	K_d (10^{-9} M)
human uPA	5.6 ± 2.8	4.4 ± 0.5	0.79	8.5 ± 3.2	315 ± 7	37
mouse uPA	0.89 ± 0.59	48 ± 19	54	4.3 ± 2.2	3.5 ± 1.2	0.81
AE120	4.4 ± 2.4	2.5 ± 0.3	0.57	no binding detected[b]		

[a] The following ligands were immobilized on the biosensor by amine coupling: human uPA, murine uPA, and AE120. Real time binding kinetics were recorded at 5 °C for injections of 2-fold dilutions of mouse or human uPAR (1 μM to 0.25 nM). [b] No binding detectable using receptor concentrations up to 1 μM.

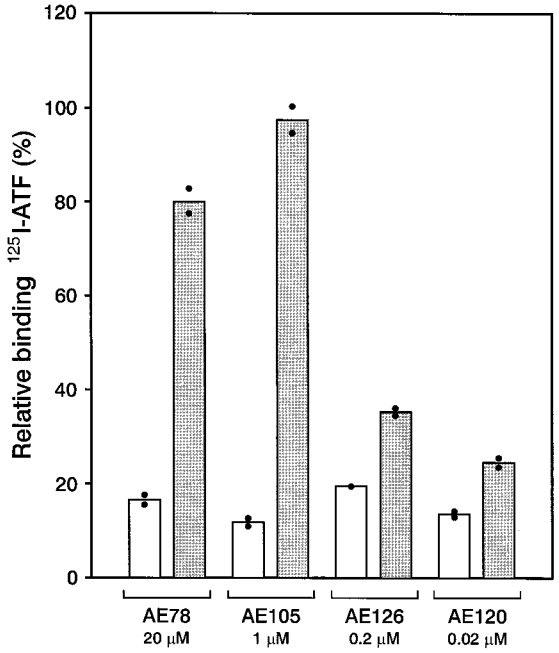

FIGURE 3: Serum stability of antagonist. To test the serum stability of selected antagonists, these were added to freshly prepared mouse serum at the following concentrations and incubated at 37 °C for 24 h: AE78 (200 μM), AE105 (10 μM), AE126 (2 μM), and AE120 (0.2 μM). The residual inhibitory activities of these antagonists were subsequently measured in the cellular binding assay after a 10-fold dilution in binding buffer (dark gray columns) and compared to the respective antagonists diluted in binding buffer with no preceding incubation at 37 °C (light gray columns). Results are presented relative to appropriate buffer controls as means (bars) and actual data points (filled circles).

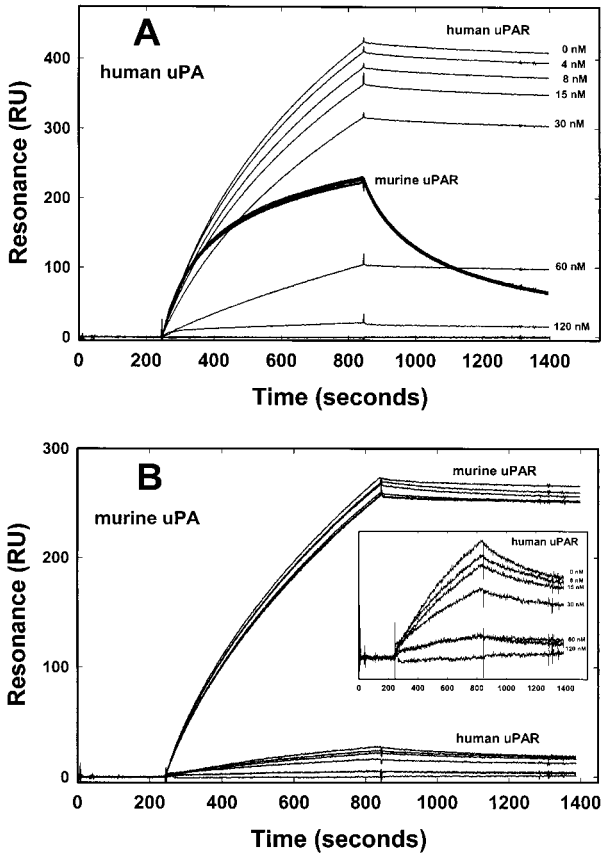

FIGURE 4: Species specificity of the antagonizing properties of AE120. Human uPA (panel A) or murine uPA (panel B) were immobilized on the sensor chip by amine coupling, and the real time binding kinetics were recorded for either 50 nM human uPAR or mouse uPAR preincubated with various concentrations of AE120 (0−120 nM). Only interactions involving human uPAR were sensitive to AE120, the concentrations of which are shown to the right of each binding curve. Since the low k_{on} values for the interaction between human uPAR and immobilized mouse uPA (Table 5) give rise to a rather weak response in surface plasmon resonance, these sensorgrams are shown at an appropriate sensitivity in the inset.

application of these peptide antagonists as lead compounds in the development of a receptor-targeted anti-invasive cancer therapy, since efficacy of such drug candidates often requires validation in mouse model systems. Consequently, we have determined the binding kinetics for the interactions between uPA−uPAR as well as AE120−uPAR using both purified human and murine components. As shown in Table 5, the reported species selectivity of the uPA−uPAR cellular interaction is further substantiated by the present kinetic data obtained by surface plasmon resonance using unlabeled, purified proteins. The interaction between uPAR and AE120 exhibits an even greater specificity, since human uPAR binds immobilized AE120 with high affinity ($K_d \approx 0.6$ nM), whereas a specific binding to purified mouse uPAR remained undetectable even at 1 μM (Table 5). Consistent with this observation, it was demonstrated in competition experiments that AE120 could compete the high-affinity interaction of human uPAR with human uPA as well as its low-affinity interaction with mouse uPA (Figure 4). In contrast, neither the high-affinity interaction of mouse uPAR with mouse uPA nor the low-affinity interaction with human uPA could be competed for by AE120 (Figure 4). To further elaborate on the species specificity of this peptide antagonist, we also tested its binding to hamster uPAR. In a cell-binding experiment similar to that shown in Figure 2C, AE120 was unable to compete for the previously reported high-affinity interaction between ^{125}I-labeled human ATF and Chinese hamster ovary cells (*49*). This extreme specificity also extended to uPAR from a nonhuman primate, as similar data were obtained using COS cells from the African green monkey (data not shown).

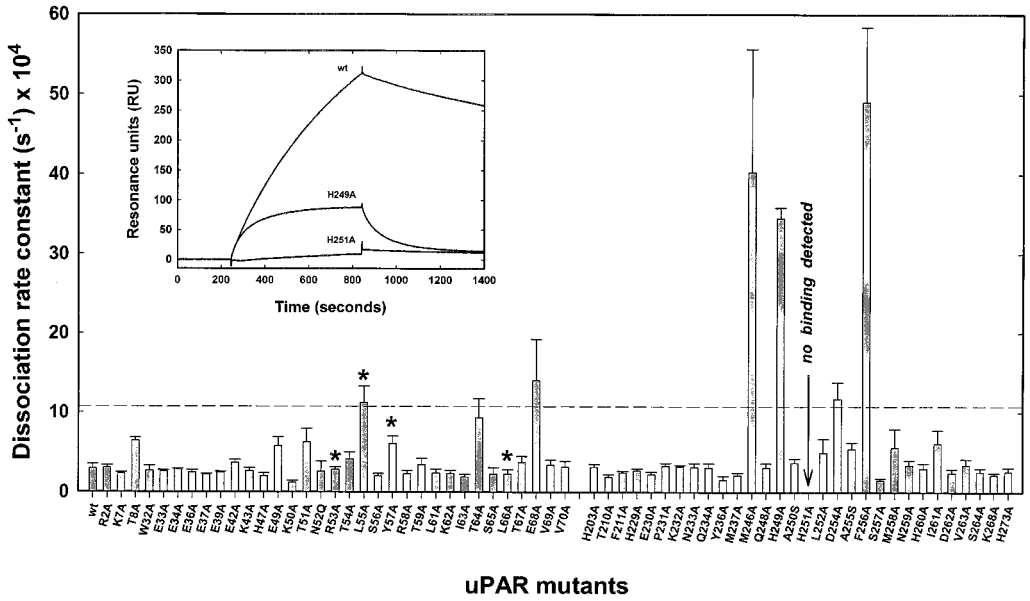

FIGURE 5: Dissociation rate constants for the interaction between immobilized AE133 and various suPAR variants carrying single-site mutations. The linear peptide antagonist AE133 (KGSGGD-Cha-srYLWS) was immobilized via its NH_2-terminal lysine residue to the biosensor chip by amine coupling chemistry (633 RU). Binding of 63 purified single-site suPAR mutants was measured in real time using surface plasmon resonance for eight different concentrations in the range of 200−2 nM. The mean of the dissociation rate constants along with its standard deviation is shown for each individual suPAR mutant. The broken line corresponds to a 5-fold increase in the dissociation rate constant compared with that of the wild-type uPAR. The asterisks identify residues previously assigned to the hot spot binding site in uPAR for uPA (*30*). The inset shows the binding profiles recorded in real time for the interactions between immobilized AE133 and wild-type uPAR (50 nM) as well as those for the single-site uPAR mutants H249A and H251A (each at 200 nM).

Identification of the Functional Epitope on Human uPAR for Antagonist Binding. To characterize the molecular basis of this unexpected strict species specificity of the affinity-matured peptide antagonist, we attempted to identify the functional epitope on human uPAR for the antagonist AE105, i.e., to locate its hot spot binding site on the receptor. The NH_2-terminally extended analogue of AE105 (AE133) was covalently immobilized on a biosensor chip by conjugation to its NH_2-terminal lysine residue, and the binding kinetics with purified human uPAR and 63 receptor mutants carrying single-site alanine substitutions located in domains I and III were measured by surface plasmon resonance (Figure 5). Only k_{off} rates were analyzed, since k_{on} values are less informative due to the influence of the restricted accessibility of the peptide in the dextran matrix (e.g., Table 4, AE133 versus AE133*). Of the 63 positions in uPAR tested by site-directed mutagenesis, 4 could be assigned to the functional epitope for the peptide antagonist (hot spot), since only these alanine substitutions either caused a >10-fold increase in k_{off} (Met^{246}, His^{249}, and Phe^{256}) or rendered complex formation undetectable (His^{251}). Minor, but significant, contributions to the free energy of antagonist binding were also noted for Leu^{55}, Glu^{68}, and Asp^{254} (Figure 5). The four critical hot spot residues are all situated in the third loop of uPAR domain III. This is consistent with previous site-specific photoaffinity-labeling studies, which demonstrate the spatial proximity of His^{251} in loop 3 of domain III and position 9 in a modified version of the parent peptide AE68 (SLNF-SQYLWS) in which the tryptophan was replaced by *p*-benzoyl-L-phenylalanine (*33*, *34*). Since the COOH-terminal region of AE68 was kept constant during the affinity maturation by combinatorial chemistry (Table 1), it is likely that the indole side chain of Trp^8 in AE105 is engaged directly in a molecular interaction with either one or more of these hot spot residues (Met^{246}, His^{249}, His^{251}, or Phe^{256}). The functional significance of this tryptophan is also emphasized by its persistence after selection in the second sublibrary (Table 2).

A sequence alignment of the relevant regions of human uPAR with those available from other species clearly demonstrates that two of the four residues assigned so far to the functional epitope for AE105 are completely conserved among these species (i.e., His^{251} and Phe^{256}), whereas the third residue (His^{249}) is unique to the human sequence and the fourth residue (Met^{246}) is shared only with uPAR from the African green monkey (Figure 6). It is therefore likely that Met^{246} and/or His^{249} have (has) a decisive role for the observed species-specific properties of the peptide antagonist. This raises the possibility that mouse uPAR may be rendered sensitive to AE105 by a limited number of mutations without affecting its high affinity for mouse uPA.

Inhibition of Human Cancer Cell Intravasation in a Chicken Chorioallantoic Membrane Model. To evaluate the effect of these peptide antagonists on cancer cell dissemination in vivo, a xenogenic model system developed to quantify intravasation of human cancer cells in chicken embryos was employed (*4*). In brief, highly malignant human squamous carcinoma cells (HEp-3), expressing both uPAR and uPA, were inoculated onto a traumatized chorioallantoic membrane in which the damaged epithelium allows almost unrestricted access to the underlying vascularized mesenchymal tissue. After 50 h of incubation, the level of intravasation by human HEp-3 cells was quantified by PCR amplification of human specific *Alu* sequences present in DNA isolated from chorioallantoic membranes processed from areas opposite to the inoculation site. Studies by anti-sense targeting have previously demonstrated that invasiveness and intravasation of HEp-3 cells in this model system are correlated to and

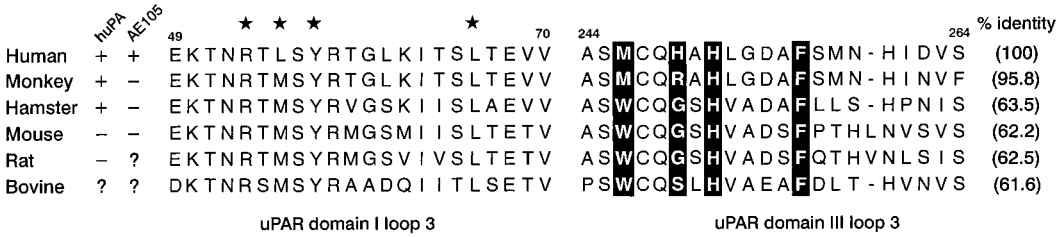

FIGURE 6: Sequence alignments of loop 3 regions in uPAR domains I and III from different species. Sequences covering loop 3 of human uPAR domains I (residues 49−70) and III (residues 244−264) are compared to the corresponding regions of the African green monkey, Chinese hamster, mouse, rat, and bovine uPAR (*18*, *49*, *54*−*57*). Sequence identities relative to full-length human uPAR are shown in brackets. Asterisks highlight residues in human uPAR important for the free energy of human uPA binding, whereas those important for binding of the peptide antagonist AE105 are shown in black boxes. Also shown is the ability of uPAR from the different species to bind human uPA and whether the peptide antagonist AE105 can inhibit this binding.

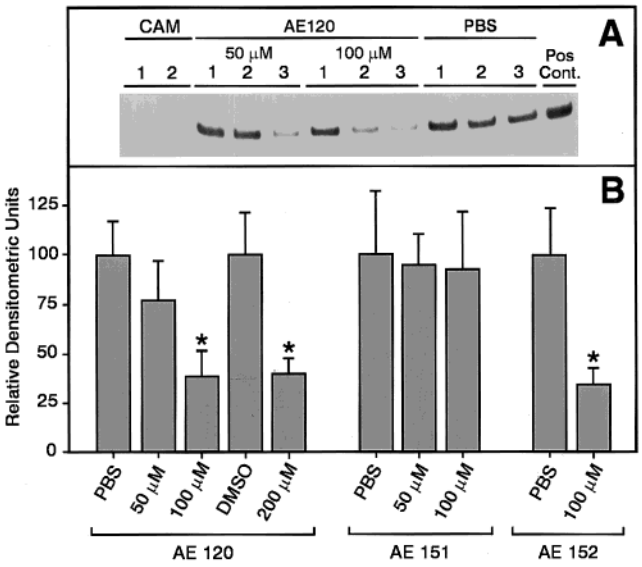

FIGURE 7: Inhibition of intravasation by the uPA-binding antagonists AE120 and AE152. Human HEp3 carcinoma cells (10^6 cells suspended in 50 μL of PBS) were inoculated on traumatized chorioallantoic membranes of chicken eggs in the presence or absence of synthetic peptides for 50 h. Additional doses of the respective peptides were administered to the inoculation site every 12 h. Shown in panel A are the 220 bp bands produced by PCR amplification of human *Alu* sequences in DNA isolated from a single set of experiments for AE120 involving nine eggs. The positive control is 1 μg of chicken DNA mixed with 10 ng of human DNA. CAM is a negative control obtained by testing DNA from chorioallantoic membranes of uninoculated eggs. The bar diagram in panel B shows quantitative, densitometric scannings of such human specific 220 bp *Alu* sequences obtained from several experiments performed on different days on a total of 54 eggs. The data are represented as means and standard errors relative to buffer controls (constituting 3−10 tests for each bar). An asterisk indicates a *P*-value less than 0.05 for a statistical comparison to the relevant buffer control using Student's *t*-test. AE120 is an antagonist of the uPA−uPAR interaction, whereas AE151 is a scrambled version thereof having no appreciable affinity for uPAR (Table 4). Due to solubility problems the highest concentration of AE120 used (200 μM) was prepared from a stock solution of the peptide in DMSO, yielding a final concentration of 0.2% DMSO in the inoculum. AE152 is a derivative of AE120 having increased solubility properties in aqueous buffers at neutral pH. It has binding kinetics similar to those of AE120 as measured by surface plasmon resonance and has the sequence [d-D-Cha-F-s-r-Y-L-W-S-D]$_2$-βA-K. In this experiment cells were cultured for 48 h in the presence of 10 μM AE152 to lower the amount of endogenously bound uPA before inoculation. DMSO is PBS containing 0.2% (v/v) DMSO.

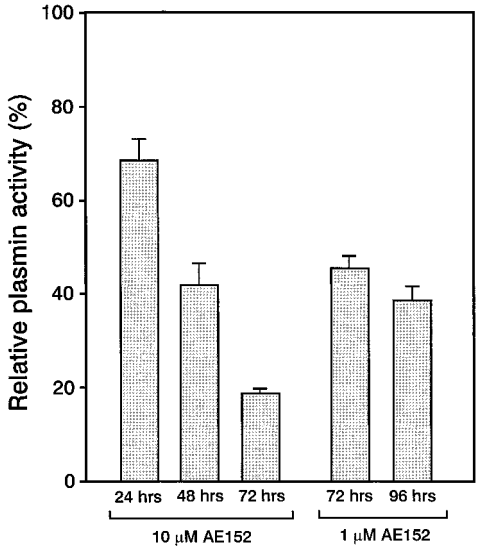

FIGURE 8: Plasmin generation by HEp-3 cells is reduced when grown in the presence of AE152. Cultures of HEp-3 cells were maintained in the presence or absence of 1 or 10 μM AE152 for various times. Culture media including inhibitor were changed daily. Cells were detached by EDTA, washed, and incubated (1×10^6 cells) with 0.6 μM plasminogen for 30 min. Aliquots of the supernatants were subsequently incubated with a chromogenic plasmin substrate to determine the level of plasminogen conversion. Data are shown relative to mock-treated cells prepared in parallel (mean and standard deviations for six determinations). In one experiment (1 μM AE152 for 72 h) the data are shown relative to cells treated in parallel with 1 μM AE151 (a scrambled inhibitor having no appreciable affinity for uPAR, Table 4).

dependent on the level of uPAR expression (*4*, *10*, *12*). As shown in Figure 7, we find in the present study that intravasation of HEp-3 cells is inhibited in a dose-dependent fashion by AE120, reaching 60% inhibition at 100 μM AE120 in the inoculation mixture. The obtained inhibitory effect is sequence specific, since no inhibition was observed using a scrambled version of AE120 having no appreciable affinity for uPAR (AE151; Figure 7).

The concentrations of AE120 needed to obtain this inhibitory effect on intravasation are relatively high compared to the high-affinity interaction with uPAR. Two properties of the intravasation assay may, however, appertain to this. First, it is almost impossible to predict the actual kinetics for the partitioning of AE120 into the chicken egg (50 mL) from such a small inoculum (50 μL), since this process, among factors, will depend on passive diffusion into the connective tissue and will be influenced by any adsorption to matrix proteins, cellular uptake, and degradation. Second, and more importantly, uPAR on HEp-3 cells exhibit a high level of saturation with endogenous uPA (approximately

90%; Ossowski, unpublished data). Since AE120 is a competitive inhibitor, it only abrogates rebinding of uPA upon dissociation as well as de novo binding of newly synthesized uPA, but it does not actively displace receptor-bound uPA. As the half-life of uPA−uPAR complexes on the cell surface is several hours (*19*, *50*), it is likely that some HEp-3 cells evade the inhibitory potential of AE120 by migration into the mesenchyme using *preexisting* uPA−uPAR complexes to breach the vessel wall, i.e., to perform intravasation. In an attempt to lower the level of saturation with endogenous uPA, HEp-3 cells were cultured in the presence of either 1 or 10 μM AE152—an active derivative of AE120 having an improved solubility in aqueous buffer. As shown in Figure 8, this treatment gradually decreased the capacity of HEp-3 cells to support plasminogen activation in vitro, but a complete abolition was not obtained. Inoculation of cells, pretreated for 48 h with 10 μM AE152, on the chorioallantoic membrane in the presence of 100 μM AE152 did, however, not cause a further reduction in the level of intravasation (Figure 7). It is therefore likely that either the residual receptor saturation with uPA is sufficient to allow some intravasation to occur or other systems also contribute to the process of intravasation, i.e., various matrix metalloproteinases.

CONCLUSIONS

Several therapeutic intervention strategies aimed at controlling the proteolytic breakdown of extracellular matrix are currently being pursued. One approach is the design of low molecular weight inhibitors specific for uPA (*51*). Another approach is the development of specific antagonists targeting the uPA−uPAR interaction (*13*−*17*). In the present study we have designed and characterized a 9-mer, nonnatural peptide antagonist of the uPA−uPAR interaction which has greatly improved receptor-binding properties compared to the original 15-mer peptide (*31*) from which it was derived by combinatorial chemistry. Two pairs of aromatic/hydrophobic side chains (Cha/Phe and Leu/Trp) were found to be critically involved in the high-affinity interaction between this 9-mer peptide antagonist and uPAR. Although this binding site has a certain structural resemblance to that present on uPA (Tyr^{24}, Phe^{25}, Ile^{28}, and Trp^{30}), these two competing ligands do not share the same functional epitope on uPAR. Residues located on loop 3 of uPAR domain I (Arg^{53}, Leu^{55}, Tyr^{57}, and Leu^{66}) are mainly responsible for the free energy of uPA binding, whereas the functional epitope for the peptide antagonist primarily resides on loop 3 in uPAR domain III (Met^{246}, His^{249}, His^{251}, and Phe^{256}). These data furthermore provide insights into the molecular mechanisms responsible for the observed species selectivity of these antagonists. To further improve our knowledge of this high-affinity interaction and to aid future rational design of uPAR antagonists, a detailed molecular description of the uPAR−peptide interface is required. The present collection of peptide antagonists provides a useful platform for the search of optimal ligands for cocrystallization studies with uPAR.

The functional impact of these uPAR-binding peptides was demonstrated in vitro by their efficiency as competitive inhibitors of human uPA binding to the human breast cancer cell line MDA-MD-231 and in vivo by their inhibitory effect on intravasation of human HEp-3 carcinoma cells in chorioallantoic membranes of chicken embryos. The application of these antagonists in mice to study their effects on tumor progression and metastasis is, however, complicated by their nonreactivity toward mouse uPAR. Consequently, genetically induced tumor models in mice are not suited for therapy studies using these inhibitors. Xenografts of human tumors on immunodeficient mice are widely used, but as there is a pronounced tumor−stroma interaction in many types of cancer, targeting of only tumor cells is unlikely to be sufficient (*52*). A metastasis model involving xenografts of human tumors on immonodeficient mice bearing a disrupted uPAR gene (*53*) may, however, prove to be of value, since these peptide antagonists inhibit the binding of both human and mouse uPA to human uPAR (Figure 4). This possibility remains to be explored experimentally.

ACKNOWLEDGMENT

We thank Helle Stærmose, Yvonne DeLotto, Charlotte Holm, Bente Johannesen, and John Post for excellent technical assistance. Nils Brünner is acknowledged for help with the mouse serum used for the stability test. The critical comments of Dr. Vincent Ellis (University of East Anglia, U.K.) are greatly appreciated.

REFERENCES

1. Andreasen, P. A., Kjøller, L., Christensen, L., and Duffy, M. J. (1997) *Int. J. Cancer 72*, 1−22.
2. Rømer, J., Bugge, T. H., Pyke, C., Lund, L. R., Lick, M. J., Degen, J. L.. and Danø, K. (1996) *Nat. Med. 2*, 287−292.
3. Murphy, G., and Gavrilovic, J. (1999) *Curr. Opin. Cell Biol. 11*, 614−621.
4. Kim, J., Yu, W., Kovalski, K., and Ossowski, L. (1998) *Cell 94*, 353−362.
5. Lund, L. R., Bjørn, S. F., Sternlicht, M. D., Nielsen, B. S., Solberg, H., Usher, P. A., Østerby, R., Christensen, I. J., Stephens, R. W., Bugge, T. H., Danø, K., and Werb, Z. (2000) *Development 127*, 4481−4492.
6. Stephens, R. W., Nielsen, H. J., Christensen, I. J., Thorlacius-Ussing, O., Sørensen, S., Danø, K., and Brünner, N. (1999) *J. Natl. Cancer Inst. 91*, 869−874.
7. Ganesh, S., Sier, C. F., Heerding, M. M., Griffioen, G., Lamers, C. B., and Verspaget, H. W. (1994) *Lancet 344*, 401−402.
8. Pedersen, H., Grøndahl-Hansen, J., Francis, D., Østerlind, K., Hansen, H. H., Danø, K., and Brünner, N. (1994) *Cancer Res. 54*, 120−123.
9. Heiss, M. M., Allgayer, H., Gruetzner, K. U., Funke, I., Babic, R., Jauch, K. W., and Schildberg, F. W. (1995) *Nat. Med. 1*, 1035−1038.
10. Kook, Y.-H., Adamski, J., Zelent, A., and Ossowski, L. (1994) *EMBO J. 13*, 3983−3991.
11. Ghiso, J. A. A., Kovalski, K., and Ossowski, L. (1999) *J. Cell Biol. 147*, 89−103.
12. Yu, W., Kim, J., and Ossowski, L. (1997) *J. Cell Biol. 137*, 767−770.
13. Crowley, C. W., Cohen, R. L., Lucas, B. K., Liu, G., Shuman, M. A., and Levison, A. D. (1993) *Proc. Natl. Acad. Sci. U.S.A. 90*, 5021−5025.
14. Min, H. Y., Doyle, L. V., Vitt, C. R., Zandonella, C. L., Stratton-Thomas, J. R., Shuman, M. A., and Rosenberg, S. (1996) *Cancer Res. 56*, 2428−2433.
15. Evans, P. C., Elfman, F., Parangi, S., Conn, M., Cunha, G., and Shuman, M. A. (1997) *Cancer Res. 57*, 3594−3599.
16. Ignar, D. M., Andrews, J. L., Witherspoon, S. M., Leray, J. D., Clay, W. C., Kilpatrick, K., Onori J., Kost, T., and Emmerson, D. L. (1998) *Clin. Exp. Metastasis 16*, 9−20.
17. Li, H., Griscelli, F., Lindenmeyer, F., Opolon, P., Sun, L. Q., Connault, E., Soria, J., Soria, C., Perricaudet, M., Yeh, P., and Lu, H. (1999) *Hum. Gene Ther. 10*, 3045−3053.

18. Roldan, A. L., Cubellis, M. V., Mascucci, M. T., Behrendt, N., Lund, L. R., Danø, K., Appella, E., and Blasi, F. (1990) *EMBO J. 9*, 467−474.
19. Ploug, M., Rønne, E., Behrendt, N., Jensen, A., Blasi, F., and Danø, K. (1991) *J. Biol. Chem. 266*, 1926−1936.
20. Ellis, V., Behrendt, N., and Danø, K. (1991) *J. Biol. Chem. 266*, 12752−12758.
21. Ellis, V. (1996) *J. Biol. Chem. 271*, 14779−14784.
22. Behrendt, N., and Danø, K. (1996) *FEBS Lett. 393*, 31−36.
23. Zhou, H. M., Nicols, A., Meda, P., and Vassalli, J. D. (2000) *EMBO J. 19*, 4817−4826.
24. Appella, E., Robinson, E. A., Ullrich, S. J., Stoppelli, M. P., Corti, A., Cassani, G., and Blasi, F (1987) *J. Biol. Chem. 262*, 4437−4440.
25. Magdolen, V., Rettenberger, P., Koppitz, M., Goretzki, L., Kessler, H., Weidle, U., König, B., Graeff, H., Schmitt, M., and Wilhelm, O (1996) *Eur. J. Biochem. 237*, 743−751.
26. Ploug, M., Rahbek-Nielsen, H., Ellis, V., Roepstorff, P., and Danø, K. (1995) *Biochemistry 34*, 12524−12534.
27. Hansen, A. P., Petros, A. M., Meadows, R. P., Nettesheim, D. G., Mazar, A. P., Olejniczak, E. T., Pederson, T. M., Henkin, J., and Fesik, S. (1994) *Biochemistry 33*, 4847−486.
28. Ploug, M., and Ellis, V. (1994) *FEBS Lett. 349*, 163−168.
29. Ploug, M., Kjalke, M., Rønne, E., Weidle, U., Høyer-Hansen, G., and Danø, K. (1993) *J. Biol. Chem. 268*, 17539−17546.
30. Gårdsvoll, H., Danø, K., and Ploug, M. (1999) *J. Biol. Chem. 274*, 37995−38003.
31. Goodson, R. J., Doyle, M. V., Kaufman, S. E., and Rosenberg, S. (1994) *Proc. Natl. Acad. Sci. U.S.A. 91*, 7129−7133.
32. Tressler, R. J., Pitot, P. A., Stratton, J. R., Forrest, L. D., Zhuo, S., Drummon, R. J., Fong, S., Doyle, M. V., Doyle, L. V., Min, H. Y., and Rosenberg, S. (1999) *APMIS 107*, 168−173.
33. Ploug, M., Østergård, S., Hansen, L. B. L., Holm, A., and Danø, K. (1998) *Biochemistry 37*, 3612−3622.
34. Ploug, M. (1998) *Biochemistry 37*, 16494−16505.
35. Solberg, H., Ploug, M., Høyer-Hansen, G., Nielsen, B. S., and Lund, L. (2001) *J. Histochem. Cytochem. 49*, 237−246.
36. Rønne, E., Behrendt, N., Ellis, V., Ploug, M., Danø, K., and Høyer-Hansen, G. (1991) *FEBS Lett. 288*, 233−236.
37. Lam, K. S., Salmon, S. E., Hersh, E. M., Hruby, V. J., Kazmierski, W. M., and Knapp, R. J. (1991) *Nature 354*, 82−84.
38. Zuchermann, R., Kerr, J. M., Kent, S. B. H., and Moos, W. H. (1992) *J. Am. Chem. Soc. 114*, 10646−10647.
39. Østergaard, S., and Holm, A. (1997) *J. Pept. Sci. 3*, 123−132.
40. Furka, A., Sebestyen, F., Asgedom, M., and Dibo, G. (1991) *Int. J. Pept. Protein Res. 37*, 487−493.
41. Kussmann, M., Nordhoff, E., Rahbek-Nielsen, H., Haebel, S., Rossel-Larsen, L., Jakobsen, L., Gobom, J., Mirgorodskaya, E., Kroll-Kristensen, A., Palm, L., and Roepstorff, P. (1997) *J. Mass Spectrom. 32*, 593−601.
42. Ploug, M., Rahbek-Nielsen, H., Nielsen, P. F., Roepstorff, P., and Danø, K. (1998) *J. Biol. Chem. 273*, 13933−13943.
43. Holst-Hansen, C., Johannessen, B., Høyer-Hansen, G., Rømer, J., Ellis, V., and Brünner, N. (1996) *Clin. Exp. Metastasis 14*, 297−307.
44. Ploug, M., Ellis, V., and Danø, K. (1994) *Biochemistry 33*, 8991−8997.
45. Chen, Y., Wiesmann, C., Fuh, G., Li, B., Christinger, H. W., McKay, P., deVos, A., and Lowman, H. B. (1999) *J. Mol. Biol. 293*, 865−881.
46. Hawkins, R. E., Russell, S. J., and Winter, G. (1992) *J. Mol. Biol. 226*, 889−896
47. Lowman, H. B., and Wells, J. A. (1993) *J. Mol. Biol. 234*, 564−578.
48. Estreicher, A., Wohlwend, A., Belin, D., Schleuning, W.-D., and Vassalli, J.-D. (1989) *J. Biol. Chem. 264*, 1180−1189.
49. Fowler, B., Mackman, N., Parmer, R. J., and Miles, L. (1998) *Thromb. Haemostasis 80*, 148−154.
50. Estreicher, A., Mühlhauser, J., Carpentier, J.-L., Orci, L., and Vassalli, J.-D. (1990) *J. Cell Biol. 111*, 783−792.
51. Zeslawska, E., Scheweinitz, A., Karcher, A., Sondermann, P., Sperl, S., Stürzebecher, J., and Jacob, U (2000) *J. Mol. Biol. 301*, 465−475.
52. Rømer, J., Pyke, C., Lund, L. R., Eriksen, J., Kristensen, P., Rønne, E., Høyer-Hansen, G., Danø, K., and Brünner, N. (1994) *Int. J. Cancer 57*, 553−560.
53. Bugge, T. H., Suh, T. T., Flick, M. J., Daugherty, C. C., Rømer, J., Solberg, H., Ellis, V., Danø, K., and Degen, J. L. (1995) *J. Biol. Chem. 270*, 16886−16894.
54. Engelholm, L. H., and Behrendt, N. (2001) *Biol. Chem. 382*, 435−442.
55. Krätzschmar, J., Haendler, B., Kojima, S., Rifkin, D. B., and Schleuning, W. D. (1993) *Gene 125*, 177−183.
56. Kristensen, P., Eriksen, J., Blasi, F., and Danø, K. (1991) *J. Cell Biol. 115*, 1763−1771.
57. Rabbani, S. A., Rajwans, N., Acharou, A., Murthy, K K., and Goltzman, D. (1994) *FEBS Lett. 338*, 69−74.

BI010662G